corrosion and materials degradation

MDPI

Article

Impact of the Delay Period between Electrochemical Hydrogen Charging and Tensile Testing on the Mechanical Properties of Mild Steel

Igor A. Chaves [1,2,*], Peter J. Richardson [2], Sam Lynch [2] and Jessica A. Allen [1,2]

[1] Centre for Innovative Energy Technologies, The University of Newcastle, Callaghan, NSW 2308, Australia; j.allen@newcastle.edu.au
[2] School of Engineering, The University of Newcastle, Callaghan, NSW 2308, Australia; peter.j.richardson@newcastle.edu.au (P.J.R.); sam.lynch@uon.edu.au (S.L.)
* Correspondence: igor.chaves@newcastle.edu.au; Tel.: +61-02-4921-2006

Abstract: With escalating global regulatory pressure for countries to adhere to emission laws, repurposing existing natural gas pipelines for hydrogen-based commodities stands to be an economical solution. However, the effects of hydrogen embrittlement must be thoroughly considered for this application to avoid the unexpected catastrophic failure of these pipelines. The literature proposes several physicochemical embrittlement models. This paper reports one aspect of hydrogen embrittlement that remains to be quantified: the recovery of ductility (embrittlement) of mild steel specimens subjected to artificially accelerated hydrogen absorption via electrochemical charging as a function of time. The effects of charging duration and particularly the delay period between charging and mechanical tensile testing were investigated. Unsurprisingly, longer charging time shows a greater loss of elongation; however, a more extensive recovery of ductility correlated with longer charging time in the first few days after charging. The data also show that while the uncharged mild steel met all minimum required values for strength and elongation for the specified grade, there was a substantial variability in the elongation to failure. The same trends in variability of elongation translated to the hydrogen-charged specimens. Due to this extensive variability, failure to meet the elongation specification of the grade is reported based on the worst-case scenario obtained for a given set of samples for each exposure condition. These results have practical implications for the monitoring and testing of infrastructure exposed to hydrogen, particularly as this relates to industry planned operational shutdown schedules.

Keywords: hydrogen charging; electrochemical charging; embrittlement; mild steel; pipeline

Citation: Chaves, I.A.; Richardson, P.J.; Lynch, S.; Allen, J.A. Impact of the Delay Period between Electrochemical Hydrogen Charging and Tensile Testing on the Mechanical Properties of Mild Steel. *Corros. Mater. Degrad.* **2024**, *5*, 265–275. https://doi.org/10.3390/cmd5020011

Academic Editor: Henryk Bala

Received: 8 April 2024
Revised: 7 May 2024
Accepted: 14 May 2024
Published: 17 May 2024

1. Introduction

The hydrogen-induced embrittlement of steel is a known phenomenon caused by the microstructural absorption of hydrogen atoms [1]. Internal microstructural blistering [2], hydrogen-enhanced localized plasticity [3], hydrogen-enhanced decohesion [4], and internal pressure theory [5] are examples of proposed physicochemical embrittlement models. Regardless of the underlying mechanisms, the operational limit state design of various types of hydrogen transport and storage infrastructure relies on standardised material properties [6,7]. The degradation of such mechanical properties with time is therefore of interest.

Several studies have focused on identifying embrittlement-resistant alloyed steels, which have successfully mitigated the effects of hydrogen embrittlement for new instalments [8–12]. However, with escalating global regulatory pressure for countries to adhere to greenhouse gas emission reduction laws [13], repurposing existing natural gas mild steel pipelines for hydrogen-based commodities stands to be an economical solution compared to costly specialised alloys, despite technical, legal, and policy considerations [14].

Factors affecting the hydrogen-induced degradation of mild steel pipelines and their connections have recently been comprehensively reviewed [15,16] and experimentally investigated for different permutations of charging solutions and materials [17,18], with electrochemical cathodic charging being the recommended method for mechanical property investigation due to its relative simplicity, accelerated exposure, and convenience [17,19,20]. Regardless of charging conditions, which vary considerably, one aspect that must be quantified is the effect of the delay between electrochemical charging and tensile strength tests of mild steel specimens. It has been known since the late 1800s that hydrogen-embrittled steels recover their ductility over the course of "days" at room temperature, with the cause attributed to the release of hydrogen gas from the metal [1]. Many modern scientific experiments and analytical techniques involving hydrogen dissolved into metal structures (including the case of hydrogen embrittlement) consider this fact and aim to reduce the loss of hydrogen either by performing in situ tensile testing [19,20], minimizing the time between exposure and testing (e.g., to <3 min [17]), or by handling specimens within cryogenic sample holders. However, none of these methods to mitigate hydrogen loss are feasible for the collection and testing of exposed samples in an industry context to provide an accurate understanding of the operational state of embrittlement. In these cases, often there are many days between the removal of a specimen and its transport to a testing facility for analysis. By that time, some loss of hydrogen, and correspondingly recovery of ductility, should be expected. There do not appear to be any accounts of documented systematic studies in the current literature which report on the effects of this delay between hydrogen exposure and tensile testing. Thus, this paper reports on the empirically quantified mechanical property degradation of mild steel specimens subjected to different charging times, and with different delay periods between hydrogen charging and tensile testing [21].

2. Materials and Methods

All test specimens were fabricated from commercially available grade 250 certified to Australian New Zealand Standard AS/NZS 3678 mild steel flat bars [22] with a nominal width and thickness of 20 mm and 5 mm, respectively. Guillotined sections 200 mm in length were machined into dog-bone test specimens by CNC according to Australian Standard methods [21]. The schematic and dimensions for the dog-bone specimens are provided in Figure 1 and Table 1, respectively.

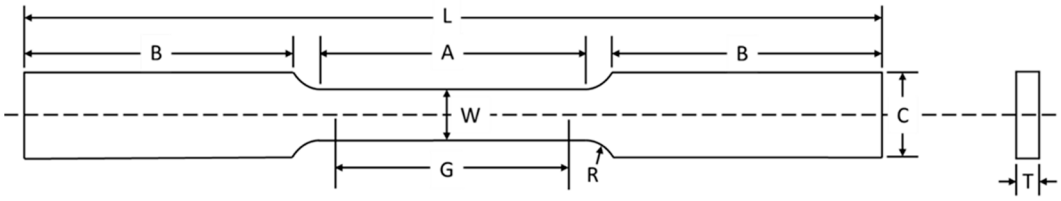

Figure 1. Schematic of AS1391:2020 dog-bone test specimens.

Table 1. Dimensions of dog-bone test specimens in mm.

L	B	A	W	G	R	C	T
200	62.5	60	12	50	20	20	5

As-received surface mill scale was removed by acid-pickling the dog-bone specimens for 2 h in a 5 M HCl solution with 3.5 g/L hexamine as a steel-corrosion inhibitor [23]. After pickling, the specimens were thoroughly rinsed with water followed by ethanol and immediately dried with a paper towel and placed in an oven until completely dry. They were then transferred to a desiccator, where they remained until they were subjected to electrochemical hydrogen charging.

For the accelerated electrochemical hydrogen charging of specimens, an electrolyte solution was prepared with 0.5 M H_2SO_4 and 5 g/L thiourea (pH of 0.3) [17]. The thiourea was selected to promote the absorption of hydrogen atoms into the steel specimen, rather than allow the recombination of hydrogen on the specimen surface to its gaseous molecular form, as has been used in previous works [17]. Additionally, 0.5 M H_2SO_4 was selected as the electrolyte due to its aggressive hydrogen embrittlement behaviour compared with other electrolytes, again as noted in previous works [17]. This allowed for a more time-efficient charging process to achieve significant amounts of as-charged embrittlement. An initial 15 min purge of electrolytes in the electrochemical cell with nitrogen gas was performed to remove any dissolved oxygen from the electrolyte solution, with continued nitrogen bubbling at a low rate throughout the charging to ensure consistency between individual specimen charging. Each dog-bone specimen was cathodically charged as the working electrode (WE) at ~6 mA/cm^2 current density with a BioLogic SP-150 potentiostat(Seyssinet-Pariset, France). Possible changes to the solution over extended periods of time were considered. It was found that for the electrolyte volume to specimen surface area ratio of 5, specimen material, and other test conditions outlined above, replacing the electrolyte with fresh solution after three individual tests was sufficient to ensure consistency, as determined by the constant-measured cell potential and current.

Figure 2 depicts a schematic of the charging cell, and Table 2 summarises the various charging times and delays to mechanical testing that were investigated. The electrochemical charging setup consists of a platinum wire-mesh counter electrode (CE) and Ag/AgCl reference electrode (RE). Generally, in electrochemical testing, the counter electrode of a three-electrode cell should be sized to be 2–3 times larger than the working electrode to ensure current limitations are not placed on the working/test electrode. In this case, the current was controlled (galvanostatic) to be maintained by the counter electrode, and potential against a reference was measured only to ensure consistency between the sample runs. The potential was found to be highly reproducible and did not vary significantly between repeated runs, reaching a stable value which did not fluctuate even for extended duration tests.

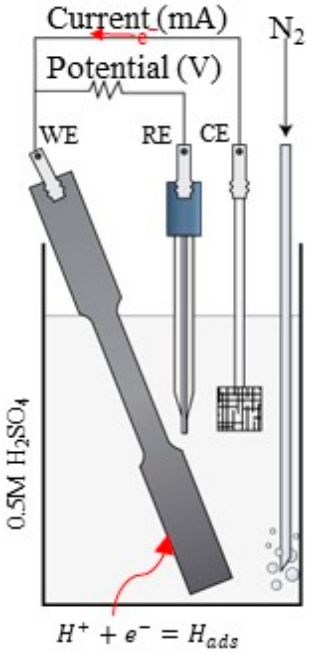

Figure 2. Schematic diagram of accelerated hydrogen-charging cell. Electron flow direction and surface where hydrogen formation occurs indicted with red arrows.

Table 2. Conditions for electrochemical hydrogen charging and delay to testing.

Charging Time (h)	Delay to Testing
0 (control)	N/A (control)
6	30 min
24	30 min
24	7 days
24	14 days
24	28 days

With consideration given to the expected strength of the grade 250 mild steel specimens (chemistry in wt%: <0.22 C, <0.5 Si, 1.7 Mn, <0.04 P, <0.03 P, <0.25 Cr, <0.3 Ni, <0.4 Cu, <0.08 Mo, <0.1 Al, <0.04 Ti, <0.02 Nb, <0.05 V, balance Fe) [22] and specimen size, tensile testing was conducted using an electromechanical Universal Testing Machine (Materials Testing Systems, MTS, Auckland, New Zealand) with 300 kN capacity. The tests were collected in displacement-controlled mode (1 mm/min) with a 0.5% applied load sensitivity. A 50 mm gauge length extensometer (0.05 mm sensitivity) was attached to the reduced thickness parallel section of the individual dog-bone test specimens and force–displacement data were collected at a rate of 10 Hz. Mechanical properties (elastic modulus, yield strength, ultimate strength, and elongation to fracture) were measured for all individually tested dog-bone specimens [24]. The elastic modulus was calculated as E = Δstress/Δstrain; the gradient was within the linear elastic region. Yield strength was determined by the upper yield stress, located at the start of or within the plastic yielding region. Ultimate tensile strength was the maximum stress experienced. Elongation to fracture was the total strain experienced before fracture, where fracture is defined as either a sudden drop to zero stress or a gradual decline in the applied stress to within 10% of the ultimate tensile stress. In all instances, with the minor exception of elongation, which is elaborated upon later in the paper, the error bars included for the results reflect the standard error calculated for each identical triplicate set of specimens.

Specimens for each charging condition (outlined in Table 2) were tested in identical triplicate to account for variability. Immediately after test specimens were tested to failure, the two fracture faces were rinsed with ethanol, dried by forced air, and placed into a desiccator for further examination.

3. Results

The combined stress–strain plots for all control (non-charged) and electrochemically charged dog-bone specimens are shown in Figure 3. Isolated triplicate stress–strain plots for each charging/delay time are organised in Figure 4.

The data for elastic modulus are shown in Figure 5 and reveal that there is an appreciable amount of variability between samples. However, it is noted that there does not appear to be any relationship between charging condition and elastic modulus. Nor do the differences in elastic modulus between specimens follow the trends observed for the hydrogen-charging-induced loss of ductility. The variation is therefore deemed to be natural and not corresponding to the charging treatment. It is noted that there is no specified minimum elastic modulus for grade 250 steel. As shown in Figures 6 and 7, respectively, the yield strength and tensile strength were largely unaffected by the charging process. As later discussed, due to a highly elevated upper yield stress for one of the control specimens (see Figure 4a), a relatively large variation in yield strength for this sample set was recorded, as seen in Figure 6. The experimentally determined yield strength for all samples met the minimum requirements for grade 250 mild steel (280 MPa), while the minimum requirements for ultimate strength for grade 250 mild steel do not apply to material with thickness <6 mm.

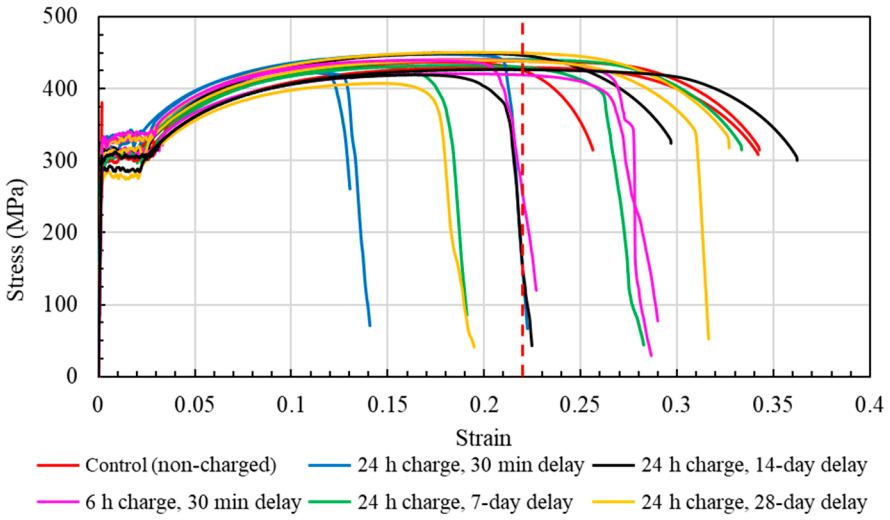

Figure 3. Combined tensile stress–strain plots for control and electrochemically charged specimens. Red-dotted line represents the specified 22% minimum elongation (strain) for grade 250 mild steel.

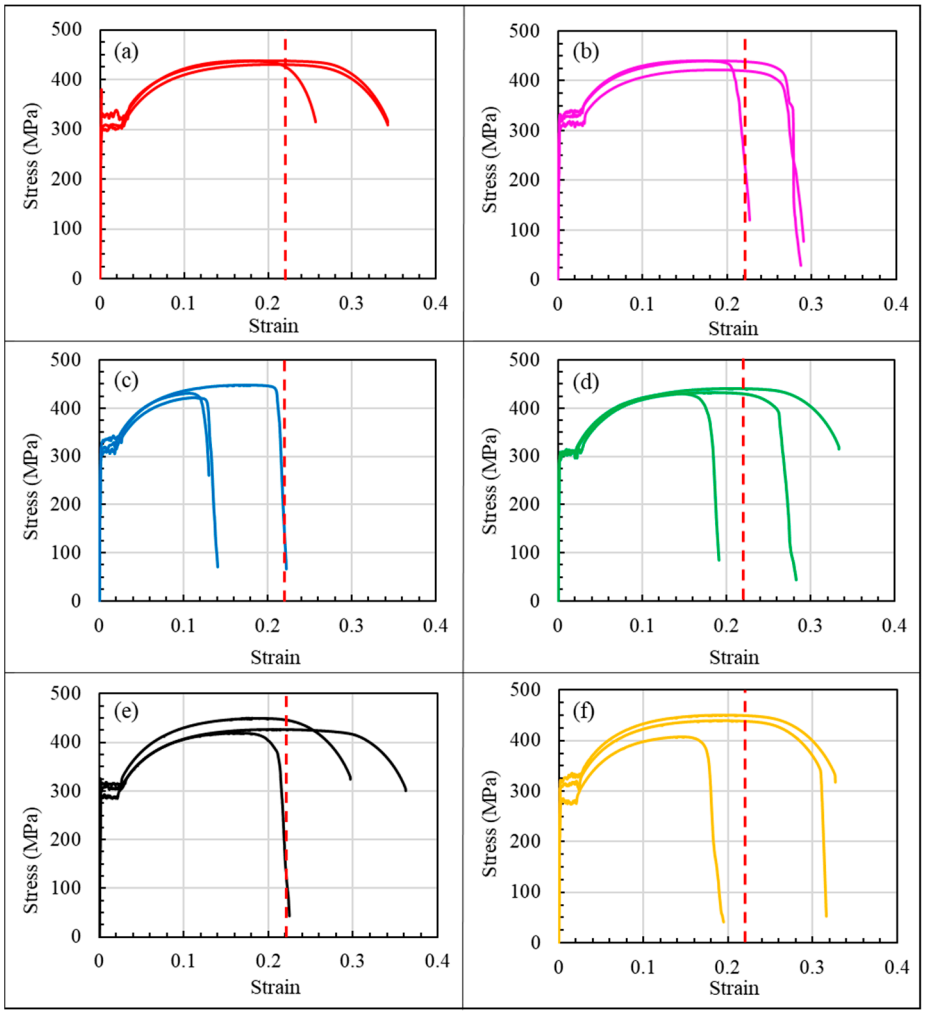

Figure 4. Triplicate stress–strain plots for various charging times and delay between end of charging and start of tensile testing: (**a**) control/non-charged, (**b**) 6 h charge, 30 min delay, (**c**) 24 h charge, 30 min delay, (**d**) 24 h charge, 7-day delay, (**e**) 24 h charge, 14-day delay, (**f**) 24 h charge, 28-day delay. Red-dotted line represents the specified 22% minimum elongation (strain) for grade 250 mild steel.

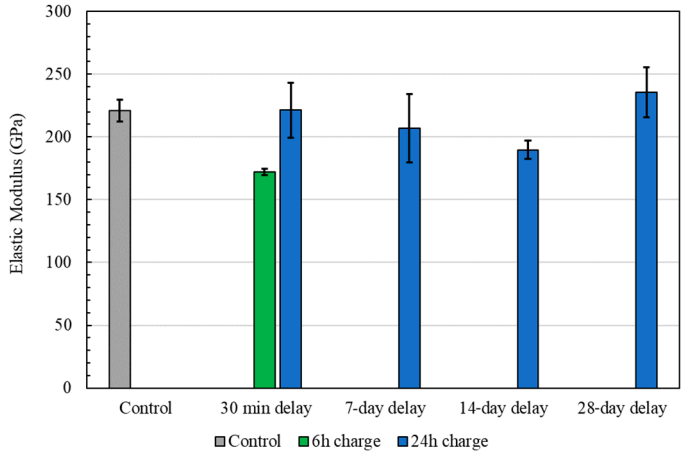

Figure 5. Average elastic modulus, including standard error bars, of identical triplicate dog-bone test specimens subjected to various charging and delay to testing times. Non-charged control specimens also shown for comparison.

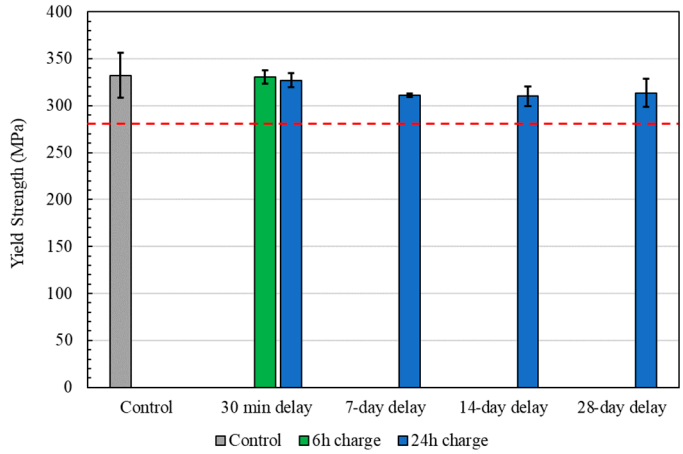

Figure 6. Average yield strength, including standard error bars, of identical triplicate dog-bone test specimens subjected to various charging and delay to testing times. Non-charged control specimens also shown for comparison. Red-dotted line represents the specified 280 MPa minimum yield strength for grade 250 mild steel.

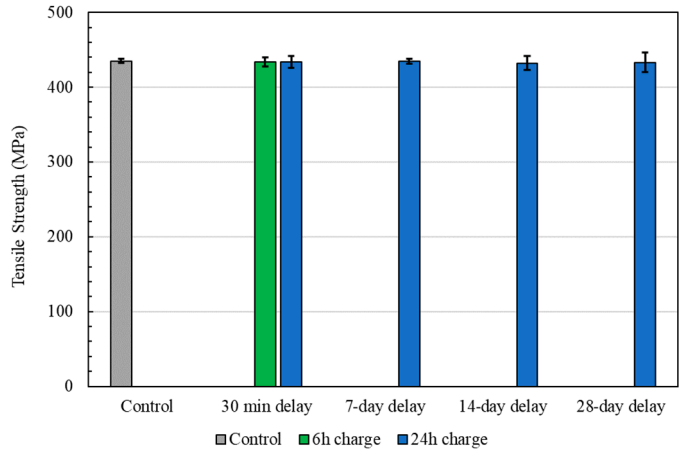

Figure 7. Average ultimate tensile strength, including standard error bars, of identical triplicate dog-bone test specimens subjected to various charging and delay to testing times. Non-charged control specimens also shown for comparison.

The elongation to failure was determined as the strain measured at the point just prior to when the applied force fell to below 10% of the maximum applied force [24]. Figure 8 shows a clear reduction in elongation for charged specimens, with the embrittlement effect being most prevalent, unsurprisingly, for the 24 h charge regime with 30 min delay to testing. It also shows that elongation was mostly recovered within the 7 days post-exposure, with diminishing and variable elongation recovery for subsequent delay periods up to 28 days.

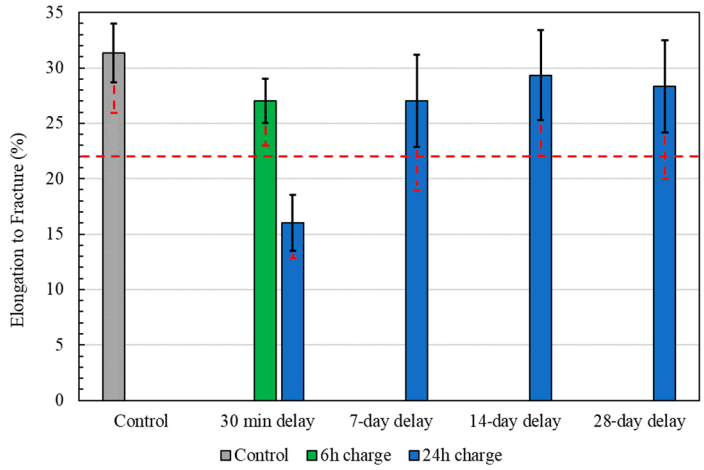

Figure 8. Average elongation to fracture, including standard error bars, of identical triplicate dog-bone test specimens subjected to various charging and delay to testing times. Non-charged control specimens also shown for comparison. Extended lower portions to each error bar denoted with red-dotted lines refer to the minimum elongation measured in each triplicate set.

4. Discussion

4.1. Variability

Variability was extensively observed for the elongation to failure of all specimens, including control (non-charged) specimens (Figures 3, 4 and 8), but care must be taken to interpret this. As per the AS/NZS standard, only a lower limit (22% for grade 250 with thickness <20 mm) is enforced for elongation [6,7]. Thus, if a sample meets this minimum elongation requirement, it can be classed as acceptable for use. This is also the case for a sample that presents elongation well beyond the acceptable limit. This implies that there may be inherent but acceptable amounts of defects and/or imperfections in a material, and that these are compensated for within the acceptable standard limits.

It is most relevant to consider the worst case or value in any given data set. Meaning, the sample with highest loss of elongation can be taken as the design consideration of the set and must meet the standard requirement for this grade (22%) for all samples within the exposure condition to meet the grade. For the control specimens, the individual sample with the lowest elongation (26%) met the standard requirement. However, as per Figure 4, considering the blue (24 h charge, 30 min delay), green (24 h charge, 7-day delay), and yellow (24 h charge, 28-day delay) data sets, the worst-case specimens fell below the acceptable limit of elongation (13%, 19%, and 20%, respectively), even though the average elongation (16%, 27%, and 28%, respectively) passed the standard requirement for the 24 h, 7-day delay and the 24 h, 28-day delay cases. Therefore, in each of these cases, the entire set does not meet the standard and cannot be accepted for use. On the other hand, for the 24 h charge, 14-day delay case, all three individual elongation values (30%, 22%, 36%) met the standard requirement, albeit only just matching the criteria for acceptability. In this case, we expect it to be very likely that if more specimens were tested there would be a high probability of one of those specimens failing to reach the minimum criteria; particularly since the 24 h charge, 28-day data set failed the meet this criteria, and there is assumed to be an overall equivalent or higher degree of ductility recovery for the 28-day delay than for

the 14-day delay. Therefore, we suggest that, given the large variability between identical specimens, a larger number of replicates should be considered in further work on this matter to fully understand the expected variability within large batches of material.

As seen in Figure 8, the 24 h charge, 30 min delay specimens showed close to twice as much loss of elongation compared to the 6 h charge, 30 min delay specimens. This is an expected behaviour attributed most likely to either an increased concentration of hydrogen within the steel for the 24 h charge case, or the more rapid dissolution, outward diffusion, and recombination of hydrogen at the steel surface for the 6 h charge case. It is noted that the ductility after 24 h charging and a 7-day delay prior to tensile testing was recovered to the same level as the 6 h charging case after a 30 min delay. It is very likely that the in-operation state of the steel during the charging process, likewise for any real-world hydrogen exposure case, would experience even greater reductions in ductility. This shows the importance of in situ testing and minimizing the delay time between the removal of steel from its exposure environment and tensile testing, where the in-operation ductility must be known.

4.2. Mechanical Properties

The elastic modulus is an intrinsic material property not expected to change with traditional strengthening treatments because it is directly related to atomic bond strength. However, the local bond strength can be affected by alloying elements, including hydrogen, which impart local lattice strains due to their different atomic size and chemical bonding characteristics to the host structure. In turn, as informed by recent comprehensive studies [2,9], we postulate that a change in elastic modulus is expected to be related to the hydrogen concentration located within a steel crystal structure. However, the data provided in Figure 5 show a significant but seemingly random variability in elastic modulus between test samples. The variability within data sets is inconsistent, with some data sets exhibiting internal agreement (relatively small error bars) and other data sets showing less internal agreement (larger error bars). Further, no meaningful trends in relation to the charging and delay times can be confirmed. Therefore, in this work, we have interpreted the large fluctuations in measured elastic modulus as being related to the large variability in the mechanical performance (and thereby chemistry and associated microstructure) of the as-supplied steel.

A recent comprehensive experimental study [17] did show an increase in the yield strength of mild steel specimens after hydrogen charging; however, those tensile tests were conducted with a minimal delay time of 3 min following the removal of samples from the electrochemical charging apparatus. It is expected that this would significantly limit the outward diffusion of hydrogen from the crystal structure, meaning that the solid solution strengthening effect could be expected to translate to a measurable increase in yield strength. In the present work (see Figure 6), there is little-to-no change in the yield strength of any charged specimens with respect to the non-charged control specimens. This is taken to mean that after a 30 min delay between charging and mechanical testing, sufficient hydrogen has escaped from the steel crystal structure that solid solution strengthening effects are no longer observed and yield strength becomes fully recovered. Likewise, for the ultimate strength (Figure 7), no difference was observed between the control and charged specimens, meaning that the full recovery of any strengthening effects was once again achieved due to the loss of hydrogen from the crystal structure.

Interestingly, while the embrittlement of metals and alloys (i.e., loss of toughness and reduction in elongation to fracture) usually comes with an associated increase in strength, this was not the case in the present work. While the elongation to fracture was significantly reduced due to the hydrogen-charging process, by up to 48% for the 24 h charge, 30 min delay data set (see Figure 8), the yield strength still remained unaffected. Alternatively, it is possible that the yield strength was increased at the time of maximum embrittlement (no delay time to testing) but was fully recovered within 30 min, while at the same time the elongation to fracture was still in the active recovery period. This would point to a much faster recovery time for yield strength than for elongation to fracture. Further investigation

of the recovery rates for various mechanical properties following exposure to hydrogen is therefore required to accurately characterise the effects of delayed mechanical testing.

As seen in Figure 6, the single control test sample's initial highest yield strength led to a relatively large 5–10% standard variation in the tested control specimens. This is considered possible within the standard [6,24]. Internal microstructural blistering [2] might have occurred, and this remains to be investigated. If this was the case, it is possible that elongation recovery could occur despite the internal degradation of lattice yield strength. A similar methodical investigation of charged samples with increasing wall thickness might shed light on this aspect.

For all charged specimens, regardless of charging or delay time, cracking could be visually observed once ultimate strength was reached. The cracks initiated at the edge of the sample and propagated transverse to the applied load (horizontally) towards the opposite edge of the reduced-thickness portion of the sample. This led to most of the charged specimens eventually failing at very low applied loads. This contrasts with the control specimens which failed in a more traditional sense, with clear necking and sudden failure at higher loads.

4.3. Practical Implications

As per Figure 8, a delay of 7days or more has little effect on embrittlement recovery. This alludes, but does not guarantee, that the maximum recovery of the exposed specimens was already achieved around the 7-day mark post-charging. This remains to be compared to practical in-operation steel infrastructures which may consist of materials with different strengthening pre-treatments, alloy compositions, geometries, and, in particular, specimen thicknesses. It also must be considered with respect to scheduled maintenance or shutdown operations. Often, natural gas pipes or tank materials are continuously exposed, sometimes under high temperatures and pressures, and may be shut down for weeks at a time for routine inspection and repair. It is unclear if post-exposed metals which have recovered from embrittlement will become embrittled or recover from embrittlement at the same rate in subsequent exposures. One could suspect that the in-operation metal will become embrittled to a greater extent, and that the effect could occur faster than for previous exposure periods due to the possible permanent hydrogen–grain boundary reactions having already taken place in previous exposure cycles. However, this remains to be investigated. Importantly, the findings from these data indicate that removing sections of in-operation mild steel specimens to perform mechanical testing must be carefully considered. Unless the specimens are processed extremely quickly (<3 min following hydrogen exposure), it is likely that the results could provide an unrepresentative value for embrittlement, potentially leading to a false sense of security. Due to the rapid nature of embrittlement recovery once hydrogen exposure has ceased, our recommendation is that an in situ mechanical analysis technique appropriate for pipelines, tanks, and other hydrogen-exposed infrastructure is explored to gain an accurate understanding of the live state of embrittlement.

It is important to note that, in this study, electrochemical charging was used to generate hydrogen atoms and force them into the steel structure as an accelerated experimental analogy to that of infrastructure which is exposed to hydrogen in different ways. In practice, temperature and pressure would be the main drivers of hydrogen diffusion into steel. We acknowledge that there may be some systematic differences between the exposure environments, which should be considered in future work. However, the main objective of this study was to induce an accelerated embrittlement effect in mild steel and to quantify the recovery, if any, of its mechanical properties. Elongation to fracture, in particular, is a critical parameter for the design of hydrogen-exposed material as it determines whether a material should be considered to act, and fail, in a ductile or brittle way. This in turn dictates the levels of allowable static and cyclic loading, including expected local displacement and corresponding strain or plastic deformation (e.g., for buried pipes, due to underground Earth movement). Ductile materials are designed based

on overload conditions (i.e., yielding), meaning that as long as the yield strength is greater than the imposed stresses, the material will survive. However, brittle materials, when considered in design, are limited by susceptibility to various loading-specific fracture initiation and propagation mechanisms, which can happen instantaneously in the form of fast fracture, or gradual fracture, as in fatigue. These can occur below the yield point. This makes it inherently more difficult to calculate and predict when the failure will occur. The ability to characterise whether a material exposed to hydrogen is still ductile or if it has become brittle is therefore an essential safety consideration, with this work emphasising that great care should be taken in interpreting the data obtained for the mechanical properties of components which have been taken out of their hydrogen-exposure environment prior to conducting testing.

5. Conclusions

1. Longer charging times show a higher loss of elongation than shorter times. For these testing conditions (relatively thick specimens, 4 mm), a more extensive elongation recovery range correlated with a longer charging time in the first few days after prolonged charging.
2. Average values of elongation to failure obtained within data sets do not accurately capture the overall behaviour of the data set due to skewed (non-normally distributed) variability from pre-existing defects in the steel. The minimum standard requirements dictate that the sample with the lowest elongation in each data set should be taken to represent the entire data set for meeting the standard.
3. Regardless of charging or delay times between charging and performing the mechanical testing, yield strength and ultimate strength were not found to be affected by the ingress of hydrogen into the steel.

Author Contributions: Conceptualization, I.A.C., J.A.A. and P.J.R.; methodology, I.A.C., J.A.A. and P.J.R.; validation, P.J.R. and S.L.; investigation and formal analysis, I.A.C., J.A.A., P.J.R. and S.L.; resources, I.A.C. and J.A.A.; data curation, P.J.R. and S.L.; writing—original draft preparation, I.A.C., P.J.R. and S.L.; writing—review and editing, I.A.C., J.A.A. and P.J.R.; visualization, P.J.R. and J.A.A.; supervision, I.A.C. and J.A.A.; project administration, I.A.C. All authors have read and agreed to the published version of the manuscript.

Funding: This research received no external funding.

Data Availability Statement: The raw data supporting the conclusions of this article will be made available by the authors on request.

Acknowledgments: The authors would like to acknowledge the technical support provided by The University of Newcastle Civil Engineering Laboratory workshop for the machining of the dog-bone specimens, and use of equipment within the Centre for Innovative Energy Technologies Electrochemical Laboratory for the electrochemical charging process.

Conflicts of Interest: The authors declare no conflicts of interest.

References

1. Johnson, W.H. On some remarkable changes produced in iron and steel by the action of hydrogen and acids. *Proc. R. Soc. Lon.* **1875**, *23*, 168–179. [CrossRef]
2. Laureys, A.; Van den Eeckhout, E.; Petrov, R.; Verbeken, K. Effect of deformation and charging conditions on crack and blister formation during electrochemical hydrogen charging. *Acta Mater.* **2017**, *127*, 192–202. [CrossRef]
3. Dwivedi, S.K.; Vishwakarma, M. Hydrogen embrittlement in different materials: A review. *Int. J. Hydrogen Energy* **2018**, *43*, 21603–21616. [CrossRef]
4. Lynch, S. Hydrogen embrittlement phenomena and mechanisms. *Corr. Rev.* **2012**, *30*, 105–123. [CrossRef]
5. Murakami, Y.; Kanezaki, T.; Mine, Y. Hydrogen Effect against Hydrogen Embrittlement. *Metall. Mater. Trans. A* **2010**, *41*, 2548–2562. [CrossRef]
6. ASM Handbook. *Material Selection and Design*; ASM International: Almere, The Netherlands, 1997; Volume 20, 958p.
7. *ASME B31.12, Hydrogen Piping and Pipelines*; American Society of Mechanical Engineers: New York, NY, USA, 2024; 268p.

8. Dong, C.F.; Liu, Z.Y.; Li, X.G.; Cheng, Y.F. Effects of hydrogen-charging on the susceptibility of X100 pipeline steel to hydrogen-induced cracking. *Int. J. Hydrogen Energy* **2009**, *34*, 9879–9884. [CrossRef]
9. Pérez Escobar, D.; Miñambres, C.; Duprez, L.; Verbeken, K.; Verhaege, M. Internal and surface damage of multiphase steels and pure iron after electrochemical hydrogen charging. *Corros. Sci.* **2011**, *53*, 3166–3176. [CrossRef]
10. Laureys, A.; Depover, T.; Petrov, R.; Verbeken, K. Microstructural characterization of hydrogen induced cracking in TRIP-assisted steel by EBSD. *Mater. Charact.* **2016**, *112*, 169–179. [CrossRef]
11. Depover, T.; Laureys, A.; Pérez Escobar, D.; Van den Eeckhout, E.; Wallaert, E.; Verbeken, K. Understanding the Interaction between a Steel Microstructure and Hydrogen. *Materials.* **2018**, *11*, 698. [CrossRef] [PubMed]
12. Cauwels, M.; Depraetere, R.; De Waele, W.; Hertelé, S.; Depover, T.; Verbeken, K. Influence of electrochemical hydrogenation parameters on microstructures prone to hydrogen-induced cracking. *Nat. Gas Sci. Eng.* **2022**, *101*, 104533. [CrossRef]
13. Fetting, C. The European Green Deal. In *European Sustainable Development Network Report*; European Sustainable Development Network: Viena, Austria, 2020; 22p.
14. Jayanti, S.E.P. Repurposing pipelines for hydrogen: Legal and policy considerations. *Energy Rep.* **2022**, *8*, 815–820. [CrossRef]
15. Laureys, A.; Depraetere, R.; Cauwels, M.; Depover, T.; Hertelé, S.; Verbeken, K. Use of existing steel pipeline infrastructure for gaseous hydrogen storage and transport: A review of factors affecting hydrogen induced degradation. *Nat. Gas Sci. Eng.* **2022**, *101*, 104534. [CrossRef]
16. Kappes, M.A.; Perez, T. Hydrogen blending in existing natural gas transmission pipelines: A review of hydrogen embrittlement, governing codes, and life prediction methods. *Corros. Rev.* **2023**, *41*, 319–347. [CrossRef]
17. Zhang, P.; Laleh, M.; Hughes, A.E.; Marceau RK, W.; Hilditch, T.; Tan, M.Y. A systematic study on the influence of electrochemical charging conditions on the hydrogen embrittlement behaviour of a pipeline steel. *Int. J. Hydrogen Energy* **2023**, *48*, 16501–16516. [CrossRef]
18. Ott, B.; Delatontaine, L.; Welchert, N.A.; Dee, S.; Reza, A. Ensuring natural gas infrastructure is suitable for hydrogen service. *Process Saf. Prog.* **2023**, *42*, 213–224. [CrossRef]
19. Tiwari, G.P.; Bose, A.; Chakravartty, J.K.; Wadekar, S.L.; Totlani, M.K.; Arya, R.N.; Fotedar, R.K. A study of internal hydrogen embrittlement of steels. *Mater. Sci. Eng. A* **2000**, *286*, 269–281. [CrossRef]
20. Nagumo, M.; Nakamura, M.; Takai, K. Hydrogen thermal desorption relevant to delayed-fracture susceptibility of high-strength steels. *Metall. Mater. Trans. A* **2001**, *32*, 339–347. [CrossRef]
21. *AS 1391*; Metallic Materials—Tensile Testing: Method of Test at Room Temperature. Standards Australia: Sydney, Australia, 2020; 78p.
22. *AS/NZS 3678*; Structural Steel—Hot-Rolled Plates Floorplates and Slabs. Standards Australia: Sydney, Australia, 2016; 35p.
23. *ASTM G1-03*; Standard Practice for Preparing, Cleaning, and Evaluating Corrosion Test Specimens. ASTM International: West Conshohocken, PA, USA, 2017; 9p.
24. *ASTM 370*; Standard Test Methods and Definitions for Mechanical Testing of Steel Products. ASTM International: Conshohocken, PA, USA, 2023; 51p.